2024 IEEE/RSJ International Conference on Intelligent Robots and Systems (IROS)
October 14-18, 2024. Abu Dhabi, UAE

Design, Modelling, and Experimental Validation of a Soft Continuum Wrist Section Developed for a Prosthetic Hand

Shifa Sulaiman[1], Mehul Menon[2], Francesco Schetter[3] and Fanny Ficuciello[4]

***Abstract*— Soft continuum sections are widely used in robotic mechanisms for achieving dexterous motions. However, most available designs of soft continuum sections cannot support payload during a motion. This paper presents a development of a novel soft robotic wrist section for a prosthetic hand named 'PRISMA Hand II'. Our research focuses on various phases of development of a soft continuum wrist section, that can support a substantial payload and maintain postures of the hand. Mechanical design, fabrication, and modelling strategies adopted for developing the wrist section are described. The design of the wrist section is constructed by assembling springs, discs, and tendons. The numbers and dimensions of springs and discs are optimised using static structural analysis. Kinematic modelling and dynamic modelling of the wrist section are carried out using Geometric Variable Strain (GVS) approach based on Cosserat rod theory and a generalised coordinate method respectively. The geometric formulations involved in Cosserat rod theory guaranteed accurate and quick computations considering deformation parameters. Dynamic modelling approach also enhanced the performance of the wrist section reducing errors and computational time during real time implementations. This paper also discusses about a dynamic model based controller strategy for the wrist section and advantages of the proposed controller are proved using a comparative study with a kinematic model based PID controller. Experimental validations of motions of the fabricated wrist section employing the dynamic controller are also included in the paper.**

I. INTRODUCTION

An anthropomorphic under-actuated prosthetic hand named 'PRISMA Hand II' [1] shown in Fig. 1(a) was developed at PRISMA lab in the university of Naples, Federico II, Italy. PRISMA Hand II is a 3D printed tendon actuated hand consisted of 19 joints powered using 3 motors and weighing around 0.339 kg. Each finger except middle finger of the hand consisted of 4 joints. The thumb has 1 revolute joint and 3 flexion/extension compliant rolling joints. Index, ring, and little fingers have 1 revolute joint and 3 flexing/extension joints. The abduction/adduction joint is not provided for the middle finger. The PRISMA Hand II is capable of carrying out in-hand manipulations and grasping related activities. The fingers of the PRISMA Hand II can manipulate deformable objects using tactile/force sensors equipped on the fingers. A novel soft continuum wrist section is developed for the hand to increase motion capabilities of the hand during manipulation tasks. This paper demonstrates the procedures we adopted for developing a wrist section capable of supporting payload and dexterous motions of the PRISMA Hand II. The work included in this paper can provide insights into various fields related to the development of a soft continuum mechanism.

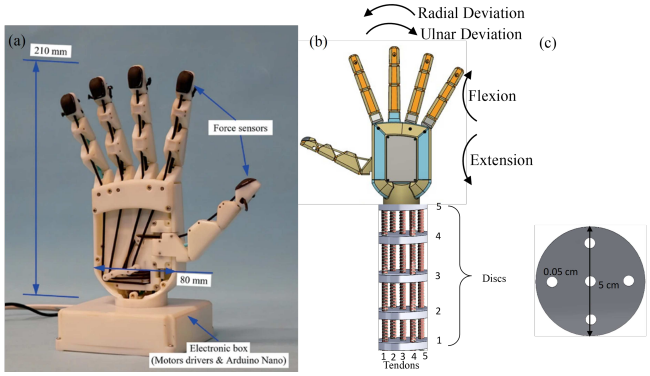

Fig. 1: Design of prosthetic hand with wrist section (a) Prisma Hand II [1] (b) Conceptual model of wrist section (c) Disc

Conceptual design of the wrist section incorporating springs, discs, and tendons for actuation is generated by considering dimensional constraints, weight, workspace, and actuating mechanisms of the hand. Kinematic and dynamic analyses of the wrist section are performed employing Geometric Variable Strain (GVS) approach and a generalised coordinate based dynamic method respectively. Final design of the wrist section is determined after analysing stress, strain, and deformation acting at different sections of the wrist under various loading conditions and tasks. Stages of fabrication and assembling of the wrist section are included in the article. A Proportional-Derivative (PD) control scheme using dynamic model of the wrist section is employed for controlling motions of the wrist section. The advantages of the proposed controller are demonstrated using a comparative study with a kinematic controller employing PID controller scheme. Errors during motion, settling time, and steady state error of two controllers are compared to determine a better controller for the wrist section. Simulation results are validated experimentally using the fabricated wrist section. The results obtained using simulations and experimental studies demonstrated the capability of the developed wrist

This work was supported by the Italian Ministry of Research under the complementary actions to the NRRP "Fit4MedRob - Fit for Medical Robotics" Grant (PNC0000007).

[1]Shifa Sulaiman is a postdoctoral researcher in the Department of Information Technology and Electrical Engineering, Università degli Studi di Napoli Federico II, Claudio, 21, 80125 Napoli, Italy ssajmech@gmail.com

[2]Mehul Menon is a Bachelor student in the Department of Mechanical Engineering, National Institute of Technology Durgapur, West Bengal 713209, India menonm98@gmail.com

[3] Francesco Schetter is a Master student in the Department of Information Technology and Electrical Engineering, Università degli Studi di Napoli Federico II, Claudio, 21, 80125 Napoli, Italy schfrn@gmail.com

[4]Fanny Ficuciello is a Faculty in the Department of Information Technology and Electrical Engineering, Università degli Studi di Napoli Federico II, Claudio, 21, 80125 Napoli, Italy fanny.ficuciello@unina.it

section to assist the motions of the hand.

Section II focuses on previous literatures related to the development of soft continuum mechanisms. Design, modelling, and fabrication of wrist section are given in section III. Section IV presents the simulation and experimental results. Conclusion of the work is given in section V.

II. Background

Development of a soft continuum mechanism is a complex task since it involves a number of analyses and procedures to finalise and implement the mechanism successfully. An efficient fabricated model finalised after undergoing modelling and analyses along with a better controller strategy is required to execute a task using a soft continuum section. In this section, some of the available developmental strategies adopted for soft robotic sections are explored.

Tendon-driven soft robotic continuum robots offer several notable advantages that enhance functionality and versatility of the whole mechanism. Their design allows for a high degree of flexibility and adaptability, enabling them to navigate complex environments and perform intricate tasks. Design of a soft continuum robot supported by springs and discs actuated using tendons was presented in [2]. The kinematic model of the robot was determined using Cosserat rod theory. Simulation and experimental studies were conducted for analysing workspace of the robot. A spring supported continuum robot actuated using tendons inspired by plant anatomy was demonstrated in [3].The kinematic model of the robot was obtained using a theoretical model of plants. The motion planning strategy for the robot was planned based on a vine inspired model by replicating oscillatory motions of the vines. A soft robotic arm made up of leaf springs, latex membrane, and discs was demonstrated in [4]. Two tendons were used for actuating the robot. Kinematic modelling of the robot was performed considering variable stiffness of the robotic structure. Modelling and control of a soft continuum robot used for navigating through thin-walled tubes using a quasi-static approach was presented in [5]. The dimensions of the tube and tension of the tendons were computed for controlling the positions of the end-effector. Dynamic model of a tendon-driven soft continuum robot using geometric exact approach was presented in [6]. Kinematic model of the robot was carried out using Cosserat model approach.

Nowadays, pneumatic actuators are used extensively for manipulating motions of soft continuum robots. A novel design of a snake like soft robot with dexterous motion capabilities actuated using pneumatic actuators was presented in [7]. The proposed snake robot can bend in opposite directions using pneumatic muscle actuators. Another novel design of a soft continuum robot actuated using pneumatic actuators was proposed in [8]. Contractions and extensions of the robot were achieved using contractor and extensor actuators respectively. A position controller was implemented for controlling the positions of the robot manipulating pressure of pneumatic actuators at no load condition. In [9], a soft robotic arm inspired from the motions of a human arm was presented. The robot can replicate the motions of the human arm using pneumatic muscles. The robot can twist and bend in multiple directions due to its unique design. Modelling of a novel soft continuum arm named 'SoPrA' employing pneumatic actuators was given in [10]. A dynamic modelling approach was integrated with proprioceptive sensors to compute external forces acting on the robot during a task. Along with pneumatic actuators, Soft Bending Actuators (SBA) are also employed to enhance the motion capabilities of soft continuum robots. Design of a soft robot using SBA made up of polyethylene material was presented in [11]. The proposed soft robotic actuator can lift a load upto 0.204 kg and capable of showcasing dexterous motions. In [7], the bending motions of a bio-inspired soft continuum arm were enhanced by employing self-bending contraction actuators. The elongation and bending motions of the top section of the robot were achieved using 4 actuators.

Payload carrying capacity of soft continuum robots are seldom explored. Payload carrying capabilities of a modular soft continuum arm were demonstrated in simulation and validated experimentally in [12]. The proposed design of the robot can grasp objects with varying geometrical and size properties. The robot was able to lift an object weighing 2 kg. Design of a hybrid robot for carrying payload with soft and rigid sections actuated using bellows was illustrated in [13]. The hybrid robot was modelled using piece-wise constant curvature model approach. A positional accuracy of about 1 cm and 5% error with respect to desired positions were obtained. A soft robot which can retract back to its initial shape was constructed in [14]. Strain gauges embedded to the robot detected the deformed state of the robot. A shape reconstruction method along with a Neural-Network (NN) based approach was used for reconstructing the shape of the robot in the presence of an external load. A novel design of a soft continuum robot constructed using a single latex rubber was demonstrated in [15]. Constant curvature based method was employed for determining kinematic model of the robot. However, experimental validations proved that the model was not capable of holding a load when the loading exceeds trunk stiffness.

A comprehensive literature review carried out related to the development of soft continuum robots shown that the current generation of soft robots has several drawbacks such as lower payload capacity, posture instability, incomplete kinematic and dynamic modelling methods, inefficient controller schemes, higher computational efforts, etc. In this paper, methods and strategies we adopted to develop a soft wrist section that can support the PRISMA Hand II's payload and dexterous motions are presented. This work attempts to build a novel soft continuum section reducing shortcomings of already available soft continuum robots.

III. Design of a soft continuum Wrist section

In this section, mechanical design, kinematic modelling, dynamic modelling, and fabrication details are included.

A. Mechanical design

Various conceptual designs of available soft robotic sections were reviewed and studied before finalising the current design of the soft robotic wrist section. The conceptual design of the wrist section was analysed in terms of load carrying capacity and range of motions in ulnar, radial, flexion, and extension directions. The structure of the wrist section was composed of discs, springs, and tendons as shown in Figs. 1(b) and (c). Stress, strain, and deformation occurred using various loading conditions were analysed for optimising the numbers, dimensions, and types of discs and springs.

The conceptual design of the wrist section for PRISMA Hand II consisted of 5 discs and 5 supporting springs (4 peripheral springs and 1 central spring) inserted through the discs. Each disc is 5 cm in radius, 5 cm in thickness, and placed 2 cm apart from adjacent discs. The number and dimensions of springs and discs were optimised using static structural analysis. Tendons inserted through the springs were manipulated for controlling motions of the wrist section. A tendon was also inserted through the central spring to enhance the stability of motions. 4 peripheral tendons were used for manipulating the rotations of the motions in 4 directions as shown in Fig. 1(b). Tendon 1 and 2 were actuated for rotating the wrist section in radial deviation direction. Similarly, motions in ulnar direction were manipulated using tendons 4 and 5. Tendons 1 and 4 were actuated for controlling motions in extension direction. Motions in flexion direction were controlled using tendons 2 and 5. The lowermost disc (disc 1) was connected to a fixed platform and uppermost disc (disc 5) was connected to the hand.

The wrist can provide a motion range of -50° to +50° in all directions with respect to the disc 5, which was sufficient for carrying out manipulation activities by the PRISMA Hand II. The wrist section was designed for carrying a payload upto 0.5 kg, since the weight of hand was 0.339 kg. The numbers and dimensions of disc, distance between discs, and properties of springs were optimised for obtaining a stable motion. Dimensions of discs were optimised using static structural analysis. Springs were selected based on the required stiffness, coil diameter, wire size, and durability.

B. Modelling of Wrist section using Geometric strain variable approach

Nowadays, different types of modelling approaches are employed for determining static and dynamic models of soft robotic links. GVS approach [16] based on a Cosserat rod model was used in this paper to model the soft robotic wrist section. The Cosserat model takes into consideration both orientation and position of the beam elements along with all six modes of deformations. Consider a soft link, j connected to a previous link, $j-1$ as shown in Fig. 2. The configuration of a soft link, j with respect to its previous link defined as a curve, $T_j(X_j)$ from 0 to L_j is given equation (1)

$$T_j(X_j)_{(0,L_j)} = \begin{bmatrix} O_j & P_j \\ 0 & 1 \end{bmatrix} se(3) \tag{1}$$

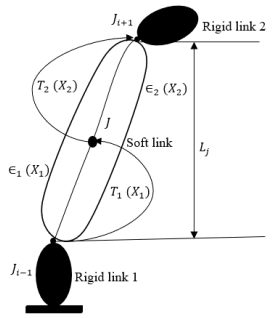

Fig. 2: Configuration of a soft link connected to a rigid link

where L_j is the length of the soft link, O_j and P_j are 3×3 orientation and 3×1 position matrices respectively. Partial derivative of soft link transformation with respect to time, $\dot{T}_j(X_j)_{(0,\ L_j)}$ is given in equation (2)

$$\dot{T}_j(X_j) = T_j\hat{\phi}_j \tag{2}$$

where $\hat{\phi}_j$ is the velocity twist of the soft link with angular velocity, ω_j and linear velocity, v_j with respect to previous body frame and is given in equations (3) and (4)

$$\hat{\phi}_j(X_j)_{(0toL_j)} = \begin{bmatrix} \omega_j & v_j \\ 0 & 0 \end{bmatrix} \in se(3) \tag{3}$$

$$\phi_j(X_j) = \begin{bmatrix} {\omega_j}^T & {v_j}^T \end{bmatrix} \in R^6 \tag{4}$$

Partial derivative of soft link transformation with respect to space, ${T_j}^{'}(X_j)_{(0,L_j)}$ is given in equation (5)

$${T_j}^{'}(X_j) = T_j\hat{\epsilon_j} \tag{5}$$

Where $\hat{\epsilon_j}$ is the strain twist of a link with angular strain, β_j and linear strain, r_j with respect to previous body frame as given in equations (6) and (7)

$$\hat{\epsilon_j}(X_j)_{(0,L_j)} = \begin{bmatrix} \beta_j & r_j \\ 0 & 0 \end{bmatrix} \in se(3) \tag{6}$$

$$\epsilon_j(X_j) = \begin{bmatrix} {\beta_j}^T & {r_j}^T \end{bmatrix} \in R^6 \tag{7}$$

The exponential representation of soft link configuration is given in equation (8)

$$T_j(L_j) = exp(\hat{\alpha_j}(L_j)) \tag{8}$$

Magnus expansion [17] is used to expand, $\hat{\alpha_j}$ along length L_j in the above equation. The relations between time derivative of the strains, velocities and accelerations of the links are given in equations (9) and (10)

$${\epsilon_j}^{'} = \dot{\phi}_j - ad_{\phi_j}\epsilon_j \tag{9}$$

$${\dot{\epsilon_j}}^{'} = \ddot{\phi}_j - ad_{\dot{\phi}_j}\epsilon_j - ad_{\phi_j}\dot{\epsilon}_j \tag{10}$$

Strain modes, $B_{\epsilon_j}(X_j)$ parameterized based on strain field, $\epsilon_j(X_j)$ with an initial strain, $\epsilon_j^*(X_j)$ and generalised coordinates, q_j are given in equation (11)

$$\epsilon_j(X_j) = B_{\epsilon j}(X_j)q_j + \epsilon_j^*(X_j) \tag{11}$$

The motions of wrist section through workspace were plotted based on GVS approach as shown in Fig. 3.

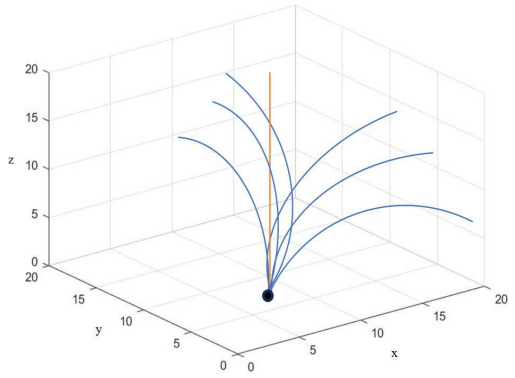

Fig. 3: Motion of wrist section obtained based on GVS approach

C. Dynamic modelling of the wrist section

The generalised dynamic equation of the soft robotic link, j with respect to generalised coordinates and vector of applied actuation forces, τ is given in equation (12)

$$M(q)\ddot{q} + C(q,\dot{q})\dot{q} + Kq = B(q)\tau + F(q,\dot{q}) \quad (12)$$

where $M(q)$ is the n x n generalized mass matrix with individual mass matrix, M_j and Jacobian matrix, J_j as given in equation (13)

$$M(q) = \sum_{(j=0)}^{N} \int_0^{L_i} J_j^T M_j J_j dX_j \quad (13)$$

$C(q,\dot{q})$ is the n x n Coriolis matrix given in equation (14)

$$C(q,\dot{q}) = \sum_{(j=0)}^{N} \int_0^{L_i} J_j^T (ad^*_{J_j} M_j J_i + M_j \dot{J}_j) dX_j \quad (14)$$

K is the n dimensional generalized stiffness (elastic force) matrix given in equation (15)

$$K = diag_{(j=0)}^{N} \int_0^{L_i} B_{\epsilon_j}{}^T \epsilon_j B_{\epsilon j} dX_j \quad (15)$$

$B(q)$ is the n x n_a (n_a is the number of actuators in the wrist section) generalized actuation matrix with internal wrench, $B_{\tau j}$ as given in equation (16)

$$B(q) = diag_{(j=0)}^{N} \int_0^{L_i} B_{\epsilon_j}{}^T B_{\tau j} dX_j \quad (16)$$

$F(q,\dot{q})$ is the vector of n x n_a generalized external forces with individual forces, F_{ej} as given in equation (17)

$$F(q,\dot{q}) = \sum_{(j=0)}^{N} \int_0^{L_i} J_j^T F_{ej} dX_i \quad (17)$$

Elasticity force and thread like actuation force equations for the internal actuators are given as follows:

$$F_{j_j}(X_j) = \sum_j (\epsilon_j - \epsilon_j^*) \in R^6 \quad (18)$$

$$F_{a_j}(X_j) = \sum_{k=1}^{na_j} \begin{bmatrix} d_{jk} t_{jk} \\ t_{jk} \end{bmatrix} \tau_j = B_{\tau j} \tau_{jk} \in R^6 \quad (19)$$

where, $d_{jk} \in \mathrm{R}^3$ represents the distance from the centre of the soft link to actuation thread, $\tau_{jk} \in \mathrm{R}^{na_j}$ is the strength of the cable and $t_{jk} \in \mathrm{R}^3$ is the vector tangent to the actuator path. Dynamic model obtained was used for determining the actuation forces required to carry out a task and aided in selecting actuators.

D. Fabrication of the wrist section

Fabrication and assembling of the wrist section to the PRISMA Hand II were carried out after finalising the conceptual model using kinematic, dynamic, and static structural analyses. The discs of the wrist section were 3D printed using Polylactic acid (PLA) material. Each tendon was connected to a motor using a coupler and the motions of tendons were manipulated to maintain stability of the wrist section. The fabricated wrist section through the manipulation of tendon force was capable to remain in a stable posture and supported the weight of the hand. The postural stability of wrist section was supported by the arrangement of discs and springs. During motion of the wrist section, the position of discs can rearrange using forces exerted by springs to maintain the posture for supporting the payload of hand. 4 stepper motors, 2 motor drivers, an Arduino mega 2560, and a 24 V converter were used for powering the wrist section as shown in Fig. 4. The properties of components used in the wrist section are given in table 1.

TABLE I: Properties of compression springs and stepper motors used in wrist section

Spring		**Motor**	
Stiffness	2.5 N/mm	Current	1 A
Coil dia.	0.5 mm	Torque	0.35 x 10^3 Nmm
Spring dia.	0.3 mm	Step angle	1.8^0
Load capacity	3.2 N	Step accuracy	± 5.0 %

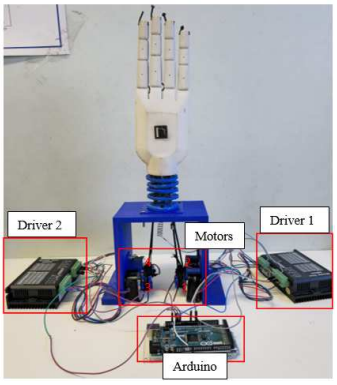

Fig. 4: Fabricated wrist section

E. A control strategy for the wrist section

A model based controller employing dynamic model was designed for controlling motions of the wrist section while traversing trajectories. The proposed controller can linearize and ensure a global asymptotic stability. Dynamic model derived in section C was used for computing generalised actuation forces related to each disc motion inside the closed

loop. The positions of discs were selected as significant points to compute generalised actuation forces. The generalised actuation forces computed with respect to each significance point were given to the soft continuum section generated inside the plant model. The output from the plant model such as output bending strain (q_{ob}) and output bending strain rate ($\dot{q_{ob}}$) were fed to the PD controller to correct the generalised actuation forces acting at each disc section. The control scheme for the wrist section is shown in Fig. 5.

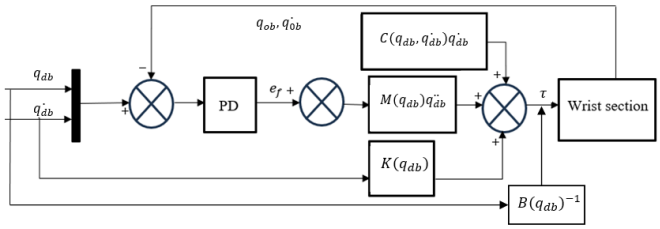

Fig. 5: Dynamic controller

Desired values of bending strain (q_{db}), bending strain rate ($\dot{q}_{db}$), and derivative of bending strain rate ($\ddot{q}_{db}$) for traversing a trajectory were computed using forward dynamic method. The desired inputs were fed to the control block as shown in Fig. 5. The desired generalised forces were given as the input to the soft robotic plant model created using Simscape soft robotic tool box. Desired generalised actuation forces, τ for each significant point for actuating tendons and errors, e_f were calculated using equations (20) and (21) respectively.

$$\tau = B(q_{db})^{-1}[M(q_{db})[\ddot{q}_{db}+e_f(t)]+C(q_{db},\dot{q}_{db})\dot{q}_{db}+K(q_{db})] \quad (20)$$

$$e_f(t) = K_P e_1(t) + K_D e_2(t)dt \quad (21)$$

where $M(q_{db})$ is the n x n non-linear mass matrix, $C(q_{db}, \dot{q}_{db})$ is the n x n Coriolis and centripetal force matrix, $K(q_{db})$ is the n dimensional stiffness term, and $B(q_{db})$ is the $n \times n_a$ actuation matrix. n x 1 vector of errors is given as follows:

$$e_f = \begin{bmatrix} e1 \\ e2 \end{bmatrix} = \begin{bmatrix} q_{db} - q_{ob} \\ \dot{q}_{db} - \dot{q}_{ob} \end{bmatrix} \quad (22)$$

IV. Results and Discussion

Design, modelling, fabrication, and control of a novel wrist section for supporting an already developed prosthetic hand are demonstrated in this paper. In the following sections, simulation study and experimental validations of the proposed strategies and comparison of the proposed controller scheme with a conventional kinematic PID based controller are presented. An experimental validation of the dynamic controller in real-time performed using a fabricated model of the wrist section to determine the efficiency of the controller was also included in this section.

A. Simulation study

Several soft robotic simulation softwares are available nowadays based on Finite Element Modelling (FEM) and Lumped Mass Modelling (LMM) approaches. However, these

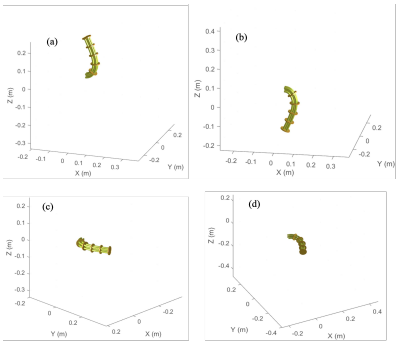

Fig. 6: Motion of wrist in x and y directions (a) Extension (b) Flexion (c) Radial deviation (d) Ulnar deviation

simulation softwares are consuming heavy computational time due to higher order of calculations during simulations. SoRoSim [18], a MATLAB based simulation software was used to simulate the motions of the soft robotic wrist section based on GVS approach. The controller loop was created inside Simulink, a MATLAB based software and the parameters computed using SoRoSim were transferred to Simulink during controlling process. Simulations were carried out on a PC with an Intelcore i7 processor and 16 GB RAM. The wrist section was assumed to be traversing trajectories in extension, flexion, radial deviation, and ulnar deviation as shown in Figs. 6 (a) - (d).

The wrist section was assumed to be moving in a range of -50^0 to $+50^0$ in ulnar deviation, radial deviation, flexion, and extension directions with respect to the last significant point on disc 5 attached to the hand. The motions of the wrist section were controlled using the proposed dynamic model based controller. Gain values (K_P and K_D) were obtained and tuned based on Particle Swarm Optimisation (PSO) technique. Desired angles and velocities corresponding to disc 5 motions were computed based on the corresponding values of bending strain and bending strain rate. The errors in motions of disc 5 obtained using simulation study for extension, flexion, radial deviation and ulnar deviation motions are shown in Figs. 7 and 8. RMSE values were determined to analyse a performance of the proposed controller. Average values of RMSE of errors in all directions of angles and velocities were obtained as 0.027 degrees and 0.031 degrees/s respectively. The RMSE values were in the tolerance range (less than 0.05) and the proposed algorithm was found efficient to control the wrist section successfully.

1) Comparison of controllers: The performance of the dynamic controller was compared with a kinematic controller developed for the wrist section as shown in Fig. 9. Kinematic equations for determining pose of the wrist section were determined using equation (1). Corrected values of angles (q_{df}) and velocities ($\dot{q}_{df}$) of significant points were determined and fed to the plant model for traversing the trajectory. A PID controller was used in the controller loop for correcting the motions. The output angles (q_o) and velocities ($\dot{q}_o$) were fed to PID controller as feedback to correct the values of input angles and velocities feeding to the wrist section. The

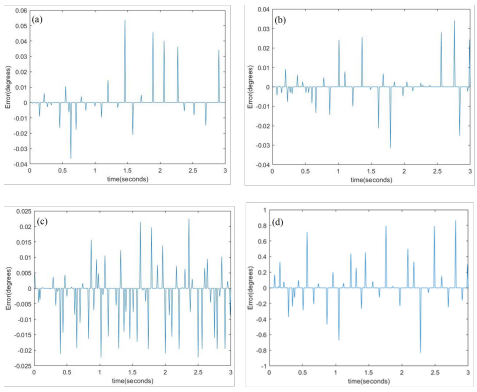

Fig. 7: Error in angles using dynamic controller (a) Extension (b) Flexion (c) Radial deviation (d) Ulnar deviation

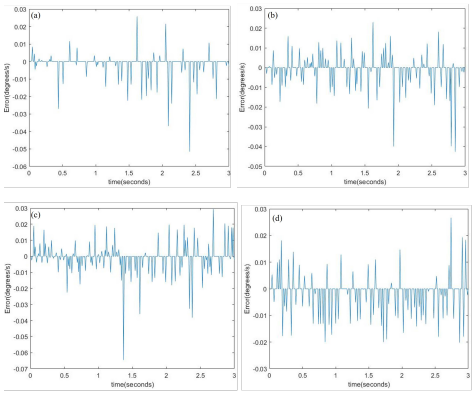

Fig. 8: Error in velocities using dynamic controller (a) Extension (b) Flexion (c) Radial deviation (d) Ulnar deviation

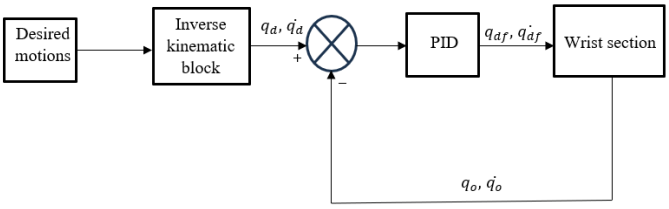

Fig. 9: Kinematic controller

errors in motions of the wrist section controlled using the kinematic controller are shown in Figs. 10 and 11. Average values of RMSE of angles and velocities in all directions were obtained as 0.241 degrees and 0.292 degrees/s respectively. The RMSE values obtained from kinematic controller were higher as compared to dynamic controller based RMSE values.

Settling time and steady state error were also compared to determine a better controller for the desired tasks as given in table 2. Settling time and steady state error during ulnar deviation, radial deviation, flexion, and extension motions of the wrist are given in table 2. The settling time and steady state error obtained using dynamic controller were found to be less as evident from table 2. The maximum values of settling time and steady state errors using dynamic controller were obtained less than 3.41 s and 0.02 degrees respectively. However, the maximum values of settling time and steady

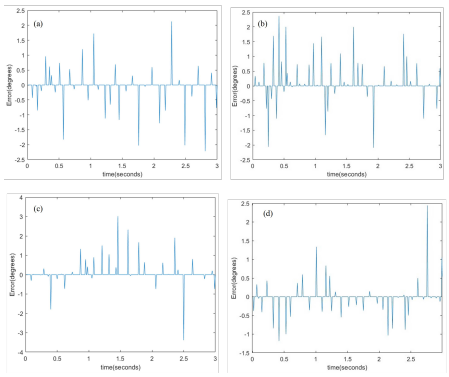

Fig. 10: Error in angles using kinematic controller (a) Extension (b) Flexion (c) Radial deviation (d) Ulnar deviation

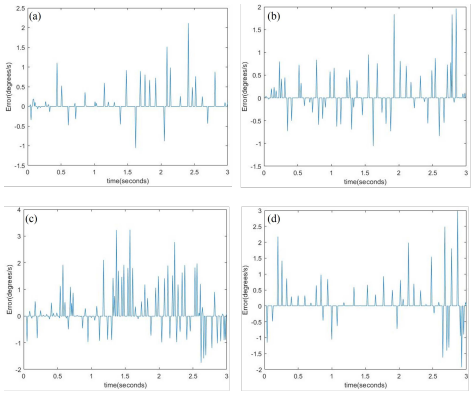

Fig. 11: Error in velocities using kinematic controller (a) Extension (b) Flexion (c) Radial deviation (d) Ulnar deviation

state error values were obtained as 5.74 s and 1.3 degrees respectively using kinematic controller strategy. Hence, the proposed dynamic controller scheme was found to be more efficient in controlling the given task with less errors.

B. Experimental validation of dynamic controller

The proposed controller scheme and motion capabilities were validated using the fabricated wrist section connected to the PRISMA hand II. An experimental set up was created by connecting the hand assembly to a platform as shown in Fig. 4. Each tendon inserted through springs were connected to a stepper motor. Wrist motions in ulnar deviation, radial deviation, flexion, and extension were validated using the experimentation. Experimentation started by maintaining all 4 tendons in a tightened stage. During ulnar deviation, motors 1 and 2 were actuated and rotated in anticlockwise (acc) direction. Motors 3 and 4 were rotated in clockwise (cc) direction in a lower phase compared to other two motors to maintain the posture of the hand and reduce actuation force acting at tendons 4 and 5. Similarly, during radial deviation motion of the wrist section, motors 1 and 2 were actuated in cc direction in a slower phase and motors 3 and 4 in acc direction in a faster phase. The wrist section can also be actuated using only two motors. Motors 2 and 4 provided motions in flexion direction and extension motions were achieved by actuating motors 1 and 3. An ArUCO marker

TABLE II: Comparison of settling time (s) and steady state error (degrees) of the dynamic controller (dc) and kinematic controller (kc)

Motion of wrist	Settling time (dc)	Steady state error (dc)	Settling time (kc)	Steady state error (kc)
Ulnar deviation	3.18	0.014	5.74	1.210
Radial deviation	3.41	0.015	5.33	1.300
Flexion	2.81	0.011	4.24	1.195
Extension	2.46	0.019	4.91	1.176

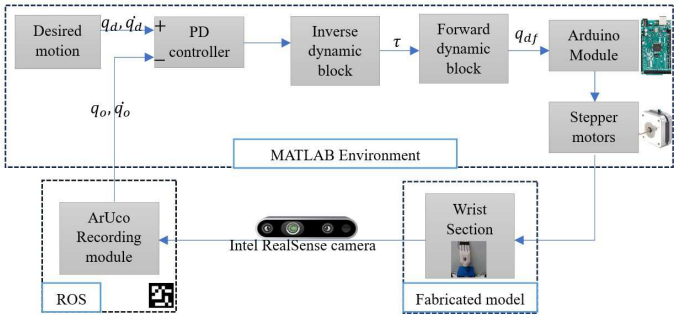

Fig. 12: Flow of data during experimentation

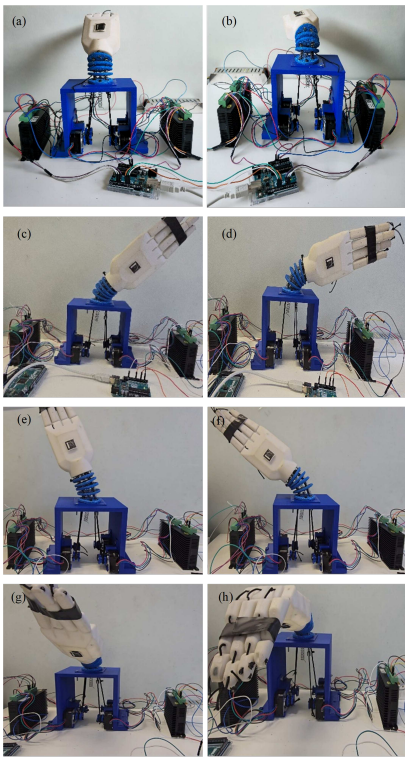

Fig. 13: Motion of wrist (a) Flexion-1 (b) Flexion-2 (c) Ulnar-1 (d) Ulnar-2 (e) Radial-1 (f) Radial-2 (g) Extension-1 (h) Extension-2

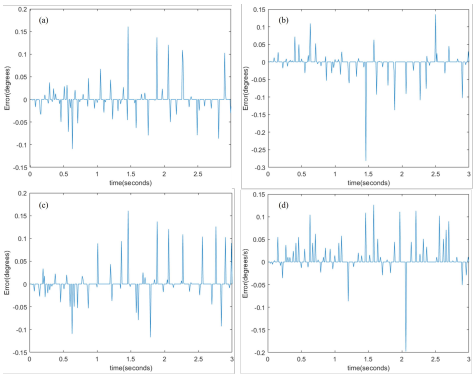

Fig. 14: Error in angles during experimentation using dynamic controller (a) Extension (b) Flexion (c) Radial deviation (d) Ulnar deviation

placed on the hand was used for tracking motions of the hand assembly during experimentation. The motions of disc 5 of the wrist section were transformed to the hand frame.

The flow of data during experimentation is shown in Fig. 12. Desired values of angles and velocities were fed to the controller scheme for computing desired generalised force values. The generalised actuation torque values were used for computing motor torque, converted to angles initially, and later updated to voltage to input to the stepper motors. The output motions of the hand tracked using ArUCO markers were fed to PD controller as feedback in forms of angles and velocities. These feedbacks were used for updating generalised actuation forces to correct the motions. An Arduino Mega 2560 and 2 microstep drivers (DM542) were used for controlling the motors. The Arduino module was connected to Simulink to transfer the computed voltage corresponding to hand motions. ROS module was used for sending ArUCO marker readings to the simulink environment. The motions of wrist section during experimentation is shown in Figs. 13 (a) - (h). Error values of angular motions and velocities with respect to desired values of bending strains and bending strain rates are shown in Figs. 14 and 15. During experimentation, RMSE values of angles and velocities were obtained in the range of 0.09 degrees and 0.07 degrees/s respectively. It is evident that the error values were higher compared to simulation study. The higher values of error were due to the springs used in the fabricated model. Continuous motions of wrist section reduced the spring stiffness and resulted in higher error values. However, the wrist section was able to carry the payload maintaining the stability of the hand during motions.

V. Conclusion and Future Works

Robotic devices often use soft continuum sections to achieve dexterous motions. Majority of soft continuum sections that are currently in the market are unable to support payload by maintaining posture while in motion. Hence, in this work we presented a novel soft continuum wrist section for a prosthetic hand named 'PRISMA Hand II' to improve mobility during manipulation capabilities. The study presented in this paper can shed light on a number of topics pertaining to the creation of a soft continuum mechanism.

The wrist section's construction, operation, and mechanical design were explained. The wrist section's kinematic

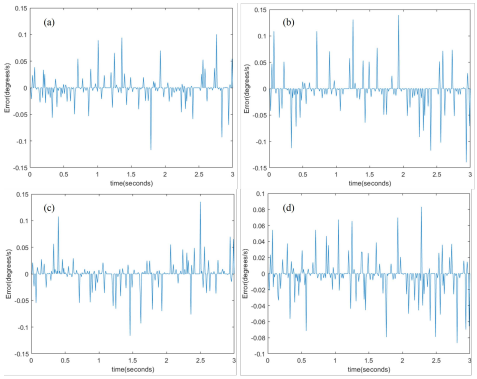

Fig. 15: Error in velocities during experimentation using dynamic controller (a) Extension (b) Flexion (c) Radial deviation (d) Ulnar deviation

modeling and dynamic modeling were completed using GVS approach and generalised force method respectively. By using the dynamic model, a PD controller scheme for controlling the motions of the wrist section was generated. The benefits of the suggested controller were demonstrated through a comparative analysis with a kinematic PID controller. This research also included experimental validations of the constructed wrist section's motions using the proposed controller. Simulation studies in SoRosim software and experimental validations using fabricated wrist section were conducted to analyse performance of the proposed soft wrist section. During simulation study, average RMSE error values of angles and velocities were obtained as 0.027 degrees and 0.031 degrees/s respectively. However, average RMSE errors of angles and velocities showcased during experimental validations were 0.09 degrees and 0.07 degrees/s respectively. The sole reason for the higher error range during experimentation was the stiffness reduction of springs employed in the wrist section. The springs will be replaced with more stable and robust supporting sections for the updations of the wrist section in future works.

According to the comparison study, RMSE errors, settling time, steady state error, and energy usage were less for the wrist motions controlled by dynamic controller. RMSE errors were more than 10% higher for the motions controlled by the kinematic controller. Settling time and steady state error using kinematic controller during the motions of the wrist section were about 10% higher. The proposed controller in this work can be integrated with an intelligent strategy to improve the performance of the wrist section along with hand performing more dexterous activities. The collision avoidance strategies of the wrist section for manipulation tasks of the hand can also be implemented for improving the performance of hand.

REFERENCES

[1] H. Liu, P. Ferrentino, S. Pirozzi, B. Siciliano, and F. Ficuciello, "The prisma hand ii: a sensorized robust hand for adaptive grasp and in-hand manipulation," in *The International Symposium of Robotics Research*. Springer, 2019, pp. 971–986.

[2] A. L. Orekhov, V. A. Aloi, and D. C. Rucker, "Modeling parallel continuum robots with general intermediate constraints," in *2017 IEEE International Conference on Robotics and Automation (ICRA)*. IEEE, 2017, pp. 6142–6149.

[3] M. B. Wooten and I. D. Walker, "Vine-inspired continuum tendril robots and circumnutations," *Robotics*, vol. 7, no. 3, p. 58, 2018.

[4] W. R. Wockenfuß, V. Brandt, L. Weisheit, and W.-G. Drossel, "Design, modeling and validation of a tendon-driven soft continuum robot for planar motion based on variable stiffness structures," *IEEE Robotics and Automation Letters*, vol. 7, no. 2, pp. 3985–3991, 2022.

[5] C. Tutcu, B. A. Baydere, S. K. Talas, and E. Samur, "Quasi-static modeling of a novel growing soft-continuum robot," *The International Journal of Robotics Research*, vol. 40, no. 1, pp. 86–98, 2021.

[6] F. Renda, M. Giorelli, M. Calisti, M. Cianchetti, and C. Laschi, "Dynamic model of a multibending soft robot arm driven by cables," *IEEE Transactions on Robotics*, vol. 30, no. 5, pp. 1109–1122, 2014.

[7] A. Al-Ibadi, S. Nefti-Meziani, and S. Davis, "Design, kinematics and controlling a novel soft robot arm with parallel motion," *Robotics*, vol. 7, no. 2, p. 19, 2018.

[8] A. Al-Ibadi, S. Nefti-Meziani, S. Davis, and T. Theodoridis, "Novel design and position control strategy of a soft robot arm," *Robotics*, vol. 7, no. 4, p. 72, 2018.

[9] A. Al-Ibadi, K. A. Abbas, M. Al-Atwani, and H. Al-Fahaam, "Design, implementation, and kinematics of a twisting robot continuum arm inspired by human forearm movements," *Robotics*, vol. 11, no. 3, p. 55, 2022.

[10] Y. Toshimitsu, K. W. Wong, T. Buchner, and R. Katzschmann, "Sopra: Fabrication & dynamical modeling of a scalable soft continuum robotic arm with integrated proprioceptive sensing," in *2021 IEEE/RSJ International Conference on Intelligent Robots and Systems (IROS)*. IEEE, 2021, pp. 653–660.

[11] S. D. Katugampala, K. M. Arachchi, S. Asanka, R. B. Arumathanthri, A. L. Kulasekera, and N. D. Jayaweera, "Design and characterization of a novel vacuum bending actuator and a bimorph: for preliminary use in a continuum robot arm," in *2019 IEEE International Conference on Cybernetics and Intelligent Systems (CIS) and IEEE Conference on Robotics, Automation and Mechatronics (RAM)*. IEEE, 2019, pp. 263–268.

[12] A. K. Mishra, E. Del Dottore, A. Sadeghi, A. Mondini, and B. Mazzolai, "Simba: Tendon-driven modular continuum arm with soft reconfigurable gripper," *Frontiers in Robotics and AI*, vol. 4, p. 4, 2017.

[13] H. D. Yang and A. T. Asbeck, "Design and characterization of a modular hybrid continuum robotic manipulator," *IEEE/ASME Transactions on Mechatronics*, vol. 25, no. 6, pp. 2812–2823, 2020.

[14] Q. Zhao, J. Lai, K. Huang, X. Hu, and H. K. Chu, "Shape estimation and control of a soft continuum robot under external payloads," *IEEE/ASME Transactions on Mechatronics*, vol. 27, no. 5, pp. 2511–2522, 2021.

[15] S. Neppalli and B. A. Jones, "Design, construction, and analysis of a continuum robot," in *2007 IEEE/RSJ International Conference on Intelligent Robots and Systems*. IEEE, 2007, pp. 1503–1507.

[16] A. T. Mathew, D. Feliu-Talegon, A. Y. Alkayas, F. Boyer, and F. Renda, "Reduced order modeling of hybrid soft-rigid robots using global, local, and state-dependent strain parameterization," *The International Journal of Robotics Research*, p. 02783649241262333, 2024.

[17] F. Renda, C. Armanini, V. Lebastard, F. Candelier, and F. Boyer, "A geometric variable-strain approach for static modeling of soft manipulators with tendon and fluidic actuation," *IEEE Robotics and Automation Letters*, vol. 5, no. 3, pp. 4006–4013, 2020.

[18] A. T. Mathew, I. B. Hmida, C. Armanini, F. Boyer, and F. Renda, "A matlab toolbox for hybrid rigid soft robots based on the geometric variable strain approach," *arXiv preprint arXiv:2107.05494*, 2021.